The bacteria-protist link as a main route of dissolved organic matter across contrasting productivity areas on the Patagonian Shelf

M. Celeste López-Abbate[1], John E. Garzón-Cardona[1,2], Ricardo Silva[3], Juan-Carlos Molinero[4], Laura A. Ruiz-Etcheverry[5,6,7], Ana M. Martínez[8], Azul S. Gilabert[1,9], Rubén J. Lara[1]

[1] Instituto Argentino de Oceanografía (CONICET-UNS), Camino La Carrindanga km 7.5, 8000 Bahía Blanca, Argentina.

[2] Departamento de Química, Universidad Nacional del Sur, 8000 Bahía Blanca, Argentina.

[3] Instituto Nacional de Investigación y Desarrollo Pesquero (INIDEP), B7602HSA, Mar del Plata, Buenos Aires, Argentina.

[4] Institut de Recherche pour le Développement (IRD), UMR248 MARBEC, IRD/CNRS/IFREMER/UM, Sète Cedex, France.

[5] Departamento de Ciencias de La Atmósfera y Los Océanos, Facultad de Ciencias Exactas y Naturales, Universidad de Buenos Aires (DCAO, FCEN-UBA), Ciudad Universitaria, Pabellón II 2do. Piso, C1428EGA Ciudad Autónoma de Buenos Aires, Argentina

[6] Centro de Investigaciones Del Mar y La Atmósfera (CIMA/CONICET-UBA), C1428EGA Ciudad Autónoma de Buenos Aires, Argentina

[7] Instituto Franco-Argentino para El Estudio Del Clima y Sus Impactos (IRL-IFAECI/CNRS-CONICET-UBA), C1428EGA Ciudad Autónoma de Buenos Aires, Argentina

[8] Instituto de Química del Sur (INQUISUR-CONICET), Universidad Nacional del Sur, 8000 Bahía Blanca, Argentina.

[9] Departamento de Geografía y Turismo (DGyT), Universidad Nacional del Sur, 8000 Bahía Blanca, Argentina.

Correspondence to: Celeste López-Abbate (mclabbate@iado-conicet.gob.ar)

Abstract

While the sources of dissolved organic matter (DOM) in the open ocean are relatively well identified, its fate due to microbial activity is still evolving. Here, we explored how microbial community structure, growth, and grazing of phytoplankton and heterotrophic bacteria influenced the DOM pool and the transformation of its fluorescent fraction. Dilution experiments were performed during the productive season on the Patagonian Shelf (SW Atlantic Ocean), a region of intense biological activity, with peak productivity observed at the shelf break front. Although phytoplankton biomass was higher than that of bacteria, protists selectively preyed on the latter, which exhibited faster growth rates, denoting trophic specificity of grazers. High trophic efficiency was suggested by the biomass distribution of protistan consumers and their prey, which predominantly exhibited a top-heavy pyramid structure. An exception to this pattern was observed at the highly productive shelf break front, where a traditional bottom-heavy pyramid emerged, indicating that most phytoplankton evaded protist predation despite evidence of herbivory. Bacterial consumption of DOM appeared uncoupled from its total amount but was influenced by DOM complexity, while the bacterial production of humic-like substances from protistan plankton precursors observed in most experiments highlighted a potential pathway for carbon sequestration. Protistan grazers also significantly influenced DOM dynamics by scaling their DOM contribution in response to the intensity of grazing on heterotrophic bacteria, regardless of productivity levels. This effect likely arises from reducing the number of active, DOM-consuming bacteria and by providing egestion DOM compounds. These findings suggest that under high bacterial growth rate that follows the onset of the productive season, protistan grazers act as a link between bacterial biomass and higher trophic levels. However, as bacterial grazing intensifies, they can simultaneously facilitate the accumulation of a fraction of DOM.

1. Introduction

Dissolved organic matter (DOM), the second-largest carbon reservoir in the ocean after dissolved inorganic carbon, is subject to dynamic regulation by physical and biological processes (Spencer et al., 2007). Unveiling the nature and dynamics of DOM is essential for gaining deeper understanding of the biochemical pathways through which carbon circulates in marine ecosystems. The optical properties of DOM serve as a marker for its sources and biological reactivity, with chromophoric DOM reflecting phytoplankton production and fluorescence DOM (FDOM) revealing potential sources and biological and photochemical interactions (Stedmon et al., 2003; Romera-Castillo et al., 2010).

Phytoplankton are primary contributors to DOM, yet processes such as viral lysis and protistan grazing also play substantial roles in shaping its composition and quantity. Protistan grazers not only recycle nutrients and enhance bloom sustainability but also impact carbon cycling through DOM production via biomass reworking and excretion (Kujawinski et al., 2004; Baña et al., 2014; Moran et al. 2022). In addition, grazers influence DOM pools by exhibiting selective feeding behaviors regarding bacterial and phytoplanktonic prey. For example, while size-specific grazing prompt compositional shifts in phytoplankton (e.g., Kanayama et al., 2020), the more generalist grazing on bacteria implies that community structure remains relatively unchanged under grazing pressure (Baltar et al., 2016). On the other hand, grazing on bacteria seems to remain close to bacterial production, specially under oligotrophic conditions (Sanders et al., 1992), while phytoplankton may temporally scape protistan grazing under favourable growth conditions thus allowing for bloom formation (Irigoien et al., 2005). This results in varying trophic transfer efficiency between phytoplankton- and bacteria-based food webs, with the former typically involving fewer carbon steps before reaching microcrustaceans (Berglund et al., 2007).

The Patagonian Shelf, one of the world's largest continental shelf regions, serves as a hotspot for carbon cycling due to its high productivity and dynamic mixing processes that connect the euphotic zone with bottom sediments (Laruelle et al., 2018). One of its defining features is a 2,500 km-long upwelling front at the shelf break, known for recurrent spring blooms and significant biogeochemical transformations that contribute to global carbon sequestration (Romero et al., 2006; Kahl et al., 2017). The emergence of an acidification trend in the water masses adjacent to the shelf is likely linked to ongoing carbon dioxide (CO_2) capture, especially in the northern area of the shelf (Orselli et al., 2018).

Given the critical roles of phytoplankton and bacteria in DOM processing and the influence of selective grazing, we conducted dilution experiments on the Patagonian Shelf during spring bloom conditions. Our study aimed to assess the fate of DOM by (i) examining the growth and grazing interactions of total phytoplankton and bacteria and (ii) tracking the chromophoric fraction of DOM and FDOM changes over time. The research spanned the mid-shelf (low to moderate productivity) and the highly productive shelf break front. We hypothesized that under conditions of moderate productivity, both bacterial- and phytoplankton-derived carbon are predominantly channeled through protistan grazing, thereby enhancing microbial loop activity. In contrast, in high productivity environments, the reduced efficiency of protists in utilizing phytoplankton biomass facilitates carbon export. We found that protistan grazing selectively targeted bacteria under both productivity regimes, and that intense grazing pressure on bacteria may contribute to the short-term accumulation of DOM

88 substances, irrespective of productivity levels. These findings enhance our understanding of the ecological
89 mechanisms influencing carbon flow in marine ecosystems.
90
91 **2.   Material and Methods**
92 **2.1   Sample collection and analyses**
93 Two groups of stations were selected in the mid-shelf (stations 23, 22 and 21 from the coast to the open ocean)
94 and the shelf break front (stations 14, 13 and 12 from the coast to the open ocean). Mid-shelf stations were
95 separated by ca. 30 km intercepting the 50 m isobath, while shelf break front stations were separated by ca. 18
96 km and intercepted the 100 and 200 m isobaths. According to the bioregionalization of the Patagonian shelf
97 waters proposed by Delgado et al. (2023), mid-shelf stations were located in low to moderate productivity
98 regions (mean chlorophyll-a concentration during the spring peak between 1.14 and 2.48 µg L^{-1}), while the
99 shelf break front stations were nested in the upwelling, highly productive region (mean chlorophyll-a
100 concentration during the spring peak of 5.8 µg L^{-1}). Hydrographic data (temperature, salinity, pressure, and
101 fluorescence) were taken with a CTD profiler SBE 9plus during the cruise H0917 from October 9 to 12, 2017.
102 Water samples for dissolved nutrients and for running the experiments were taken from the chlorophyll-a
103 maximum with 6 L Niskin bottles attached to the CTD rosette, while dissolved organic carbon (DOC) samples
104 were taken in the surface layer (5 m). The measurement of inorganic nutrients (NO_2^-, NO_3^- and NH_4^+, PO_4^{3-},
105 and Si), was carried out by analyzing 50 mL aliquots of seawater preserved with $HgCl_2$ solution (Kattner and
106 Becker, 1991). The concentration of dissolved inorganic nitrogen (DIN) was calculated as the sum of NO_2^-,
107 NO_3^- and NH_4^+. Filtered (Whatman GF/F glass fiber filters) samples for DOC were collected in pre-combusted
108 20 mL glass vials and acidified to pH < 2 with H_3PO_4. Filtrates were analyzed using high-temperature (680°C)
109 catalytic oxidation with Al_2O_3 particles containing 0.5% platinum (Pt) in a TOC analyzer (Dohrmann DC-190,
110 CA, USA). The resulting CO_2 was then quantified using non-dispersive linearized infrared gas analysis (Skoog
111 et al., 1997).
112
113 **2.2   Satellite chlorophyll-a**
114 The spring phytoplankton bloom is a recurrent feature of the Patagonian Shelf and shelf break (e.g., Delgado et
115 al., 2023). A time series of satellite-derived chlorophyll-a was constructed to capture the bloom timing at each
116 station during the sampling period. Moderate Resolution Imaging Spectroradiometer (MODIS) Aqua images
117 of chlorophyll-a concentration were downloaded from the National Aeronautics and Space Administration
118 (NASA) ocean color web site (https://oceancolor.gsfc.nasa.gov/). Daily Level 3 images with a spatial resolution
119 of 4 km were obtained for the period spanning August 2017 to December 2017, capturing the closest pixel to
120 each sampling point. To minimize the percentage of missing values, we computed the 5-day mean and applied
121 a low-pass filter to remove the variability lower than 28 days.
122
123 **2.3   Experimental setup**
124 Feeding experiments, based on the dilution technique (Landry and Hassett, 1982), were prepared by gently
125 mixing different percentages of unfiltered water and filtered water through <0.2 µm Whatman polycarbonate

126 filters. Four dilution treatments (D) were prepared using the filtered and unfiltered water: 10%, 40%, 70% and

127 100% (whole water). Water was pre-filtered by a 200 µm mesh net to eliminate larger metazoan grazers. Acid-

128 cleaned, 1 L glass experimental bottles (3 replicates) were daily (24 h) deployed at a deck-incubator (200 L)

129 equipped with continuous in situ water flow and covered with a double knitted mesh fabric (~215 g m^2) to

130 attenuate the UV radiation. Dissolved inorganic nutrients (N, P and Si) were added to the incubation bottles

131 following the recommendations by Calbet and Saiz (2018) to ensure phytoplankton growth at non-limiting

132 conditions. Assuming moderate phytoplankton growth rates and maximum chlorophyll-a concentrations of 2

133 µg L^{-1} in the mid-shelf region and 6 µg L^{-1} in the shelf break front (Delgado et al., 2023), we supplemented the

134 water with 8.3 µM of nitrogen and silicon, and 0.5 µM of phosphorus in the mid-shelf area, and 24.9 µM of

135 nitrogen and silicon, and 1.5 µM of phosphorus in the shelf break front. A series of triplicate dilution bottles

136 without added nutrients was set as control treatment.

137 Subsamples from the initial and final treatments were collected for chlorophyll-a and bacteria abundance

138 analyses. To determine chlorophyll-a, samples (300 mL) were filtered through Whatman GF/F glass fiber filters

139 and stored at -20°C. Pigments were extracted with 90% acetone for 24 h in the dark at -20° C and then

140 determined spectrophotometrically according to Jeffrey and Humphrey (1975). Heterotrophic bacteria were

141 quantified by staining 1 mL seawater sample with 4,6-diamidino-2-phenylindole (DAPI) to a final concentration

142 of 3 µg mL^{-1} and collected on black polycarbonate filters (25 mm diameter, 0.2 µm pore size). The enumeration

143 was done with a Nikon Eclipse 80i microscope equipped with a fluorescence lamp at 100X magnification and

144 using a UV excitation filter (330-385 nm). Twenty-five images were taken at random points from each

145 polycarbonate filter using a Nikon DXM1200F digital camera and subsequently, every cell in the image was

146 enumerated and sized using the software ImageJ. Bacterial cell volumes were calculated assigning simple

147 geometric shapes to species (coccos, bacillus), and converted into carbon content (µg C L^{-1}) by the allometric

148 model according to Simon and Azam (1989).

149 Plankton samples were collected from the initial treatments to characterize the community structure at the

150 starting conditions. For the analysis of plankton in the 2–5 µm size range, triplicate samples (3 mL) were fixed

151 with 0.53 mL of glutaraldehyde (f.c. 2 %) and subsequently processed following the methods described by

152 Porter and Feig (1980). The same procedure was applied for plankton in the 5–20 µm size range, using duplicate

153 100 mL samples for counting. The identification of organisms was done by a combination of light and epi-

154 fluorescent microscopy. Preserved samples were stained with DAPI (f.c. 5 µg mL^{-1}) and proflavine (f.c. 5 µg

155 mL^{-1}) and collected on black polycarbonate filters (25 mm diameter, 0.2 µm pore size). Most taxa were

156 identified using a blue excitation filter (450-490 nm) while Cryptophytes were identified using a green

157 excitation filter (480-550 nm). Cell enumeration was done by settling the preserved sample (1-2 mL) in

158 Utermöhl chambers during 24 h. The entire chamber was analyzed under a Wild M20 inverted light microscope.

159 Similarly, the enumeration of plankton in the size fraction 20-200 µm was done by settling a variable volume

160 (50–100 mL, depending on sediment and plankton concentration) of preserved water sample (Lugol's iodine)

161 in Utermöhl chambers during 24 h. It is worth mentioning that since samples were pre-filtered through a 200

162 µm mesh to exclude larger consumers from our experiments, colony-forming protists may have been removed.

163 Biomass estimation involved assigning simple geometric shapes to species to quantify cell volume, which was

subsequently converted into carbon content (μg C L^{-1}) according to Hillebrand et al. (1999). Protistan taxa abundance was visualized by a heatmap (employing the R package *heatmaply*). Heterotrophic and autotrophic taxa were segmented into groups based on size, distinguishing between nanoplankton (2-20 μm) and microplankton (20-200 μm) (Sieburth et al., 1978). Nanoplankton included heterotrophic nanoplankton (HNP), coccolithophores, and phototrophic nanoplankton (PNP), while the microplankton comprised ciliates, heterotrophic dinoflagellates (HD), phototrophic dinoflagellates (PD), and diatoms. Additionally, HNP comprised both flagellates and ciliates, while PNP encompassed dinoflagellates, diatoms, and flagellates. A side dendrogram was included to group similar sampling stations by ordering rows (stations) so that the sum of distances between each one will be minimized. Data for ranking rows was normalized to range from 0 to 1. To identify the dominant taxa contributing to station ordination, a biplot based on non-metric Multi-Dimensional Scaling (MDS) was created using the R package *vegan.*

An additional treatment of pre-filtered (Whatman GF/F glass fiber filters) and undiluted water was set to separate protists and measure the absorbance at 254 nm and FDOM. This was aimed to compare the DOM pool at the initial and final incubation conditions in the presence (i.e., in unfiltered, undiluted treatment) and in the absence of protists (i.e., in pre-filtered by 0.7 μm, undiluted treatment). Biotic effects are known to produce DOM transformations in short timescales. For instance, significant shifts in both the chromophoric and fluorescent fractions of DOM driven by biological processes were identifiable after 24 h (Urban-Rich et al., 2004; Lønborg et al., 2010; 2015), while DOM transformation driven by bacteria occurred within the first 24 h upon their release by phytoplankton (Gruber et al., 2006; Hach et al., 2020). The optical properties of FDOM were evaluated from emission-excitation matrices (EEM) obtained with a Shimadzu RF-5301 scanning spectrofluorometer with a 150 W xenon lamp and a 1 cm quartz cell. Milli-Q water was used as reference and the intensity of the Raman peak was regularly checked. The emission wavelength ranged between 250 nm and 600 nm while the excitation wavelength ranged between 220 nm and 370 nm. Dissolved humic-like and protein-like substances were estimated using the wavelengths proposed by Coble (1996). Humic-like material was represented by three fluorophores: $FDOM_C$ (Ex/Em: 350/440) and $FDOM_A$ (Ex/Em: 250/425) of terrestrial origin, and $FDOM_M$ (Ex/Em: 310/380) of marine origin. $FDOM_C$ indicates highly unsaturated components, $FDOM_A$ reflects a moderate degree of unsaturation, and $FDOM_M$ suggests a low degree of unsaturation. Protein-like material was characterized by two fluorophores: $FDOM_B$ (Ex/Em: 260/300) and $FDOM_T$ (Ex/Em: 270/330), both derived from autochthonous biogenic sources. $FDOM_B$ is associated with compounds similar to tryptophan and tyrosine, linked to recent organic matter production through primary productivity, while $FDOM_T$ indicates tryptophan-like compounds formed from microbial protein breakdown (Jørgensen et al., 2011; Drozdova et al., 2022). Fluorescence intensity of fluorophores was expressed in Arbitrary Units (AU). Fluorophores were identified using the PARAFAC multivariate algorithm (Stedmon and Bro, 2008), and different biogeochemical indicators such as humification index (HIX), fluorescence index (FI), and freshness index (BIX), were calculated (Coble, 1996). The HIX serves as a tool for assessing the diagenetic condition of DOM, as it increases with aromaticity (Bai et al., 2015), while the FI distinguishes between DOM of different origins, i.e., terrestrial vs. microbial (McKnight et al., 2001). The BIX aims to estimate the relative contribution of DOM produced in situ by microbes (Huguet et al., 2009).

202 The absorbance spectra between 240 to 800 nm were measured in a Perkin Elmer Lambda 35
203 spectrophotometer. The absorbance at 254 nm (a254) from the chromophoric fraction of DOM was used as a
204 proxy of the DOM amount (Brandstetter et al., 1996). Net changes in the a254 fraction of DOM across the
205 incubation time were calculated as $1/t \ln (a254)t/(a254)0$, where $(a254)0$ and $(a254)t$ are the a254 nm at the
206 initial (0) and final (t) conditions, respectively. Lee et al. (2018) identified parameters with more than a 50%
207 absolute percent difference between the control and treated samples as reliable indicators to distinguish between
208 DOM transformation caused by biodegradation, UV irradiance, and adsorption. Here we used the tendency
209 during incubation of BIX, HIX, FI, and the ratio between FDOM components M and A ($FDOM_M/FDOM_A$) as
210 reliable parameters for the discrimination of biodegradation versus UV photodegradation or adsorption.
211 Pairwise relationship between net changes in a254 in the presence and absence of protists with variables of
212 interest, was evaluated by simple regression models. The same procedure was used with other variables to test
213 for pairwise relationships of ecological significance.
214
215 **2.4   Phytoplankton and bacterial growth and grazing by phagotrophic protists**
216 Rate estimates of phytoplankton growth (μ) and mortality due to protist grazing (m) were obtained using the
217 equations of Landry and Hassett (1982). While initially intended for measuring phytoplankton growth and
218 mortality, we adapted this method to assess bacterial growth rate and bacterivory. This approach has been
219 demonstrated to be effective and reliable for use with natural bacterial communities in non-oligotrophic regions
220 (Tremaine and Mills, 1987). The method is based on measuring the initial and final concentration of
221 chlorophyll-a (as a proxy of phytoplankton biomass) and bacterial abundance in triplicate dilution series after
222 an incubation period of 24 h. It assumes that protistan grazing rate is a linear function of prey concentration
223 (Holling type I functional response), and can be calculated as follows:
224
225 $$\mu_0 = 1/t \ln Pt/P0 = \mu - mD$$
226
227 where μ_0 is the apparent growth rate, P0 and Pt are the phytoplankton concentration at the initial (0) and final
228 (t) conditions, respectively, D is the dilution series. The m:μ ratio x 100 was used to calculate the percentage of
229 the daily bacterial/primary productivity consumed by protistan grazers. We tested model fit by linear regression
230 analysis in every experiment.
231
232 **3.   Results**
233 **3.1   Phytoplankton phenological stages at the sampling area**
234 Mean surface chlorophyll-a, derived from satellite observations during the sampling period (October 9-12,
235 2017, Fig. 1a), revealed a band of high phytoplankton concentration at the shelf break front, centred at the 114
236 m isobath in the latitudinal band at 40°S. While the spring bloom typically begins during September in the
237 latitudinal range of our sampling area (Delgado et al., 2023), phytoplankton at the time of sampling, as estimated
238 from satellite chlorophyll-a, were at different phenological stages in each station (Fig. 1b). At the mid-shelf,
239 station 21 showed the highest concentration of satellite chlorophyll-a and the phytoplankton community was at

240 the pulse initiation. Stations 22 and 23 showed lower chlorophyll-a and were sampled at bloom stationary phase.

241 At the shelf break front, satellite-derived chlorophyll-a levels were elevated in stations 13 and 14, indicating

242 proximity to the bloom peak, whereas station 12 exhibited low chlorophyll-a concentration, corresponding to

243 the bloom termination phase.

244

245
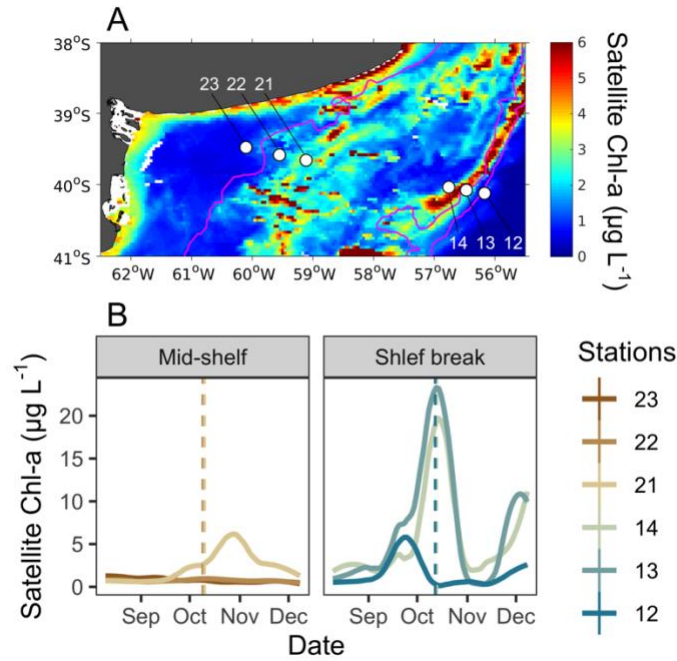
246 **Figure 1.A. Map of the study site showing the location of sampling stations (white dots) and the mean**

247 **surface distribution of satellite chlorophyll-a (Chl-a) during the sampling period (October 09-12).**

248 **Stations 23, 22 and 21 were located in the mid-shelf area, and stations 14, 13 and 12 were located in the**

249 **shelf break front. B. Temporal evolution of surface satellite Chl-a concentration at grid points closest to**

250 **sampling stations in the mid-shelf and the shelf break front. Solid lines denote satellite Chl-a**

251 **concentration at each station, while dashed lines represent the date of in situ sampling. Lines are color-**

252 **coded according to the symbols representing each station.**

253

254 **3.2   Hydrography, nutrients, and DOM properties**

255 Thermohaline signature was in the range of the Subantarctic Shelf waters ($33.5 < S < 34$) from station 21 to

256 station 14 in agreement with Berden et al. (2020) and Ferronato et al. (2023). At the mid-shelf area, station 23

257 and 22 showed relatively higher salinity values ($S > 33.7$), linked to the coastal maximum salinity waters

258 originating at San Matias Gulf (Lucas et al., 2005). These stations also showed weak stratification, while the

259 rest of the stations showed a sharper thermocline. The mixed layer depth (MLD) was shallower (10 m) in

260 stations 12 and 23, whereas in all other stations, it averaged 30 m. All samples taken at the chlorophyll-a

261 maximum were positioned within the mixed layer.

262 The concentration of dissolved nutrients (DIN, PO_4^{3-} and Si) was highest at station 12, while the lowest total

263 nutrient concentration was recorded at station 23 (Fig. 2). The primary nitrogen source was NO_3^-, except for

264 station 22 where NH_4^+ predominated. The only notable distinction between station groups was the concentration

265 of NO_3^-, which averaged 1.2 µM in the mid-shelf stations and 7.3 µM in the shelf break front stations. According

266 to Redfield ratios (Redfield et al., 1963), a strong nitrogen depletion in relation to PO_4^{3-} and Si occurred in

267 station 23. While the N:P ratio was closer to 16:1 in the rest of the stations, a general excess of PO_4^{3-} in relation

268 to DIN was registered. On the contrary, all stations except for station 23, showed a Si depletion in relation to

269 DIN. The concentration of DOC in surface waters was homogeneous in the mid-shelf stations (mean of 79 µM),

270 while in the shelf break it varied from 96 µM, in station 14, to 52 µM, in station 13 (Fig. 2). The highest

271 fluorescence intensity of protein-like compounds ($FDOM_T$ and $FDOM_B$) was found in station 23, while the

272 highest intensity of humic-like fluorophores was observed in station 21 (Fig. 3). The a254 was higher in the

273 mid-shelf stations (mean of 2.3 m^{-1}) compared to the shelf break front stations (mean of 1.3 m^{-1}).

274

275
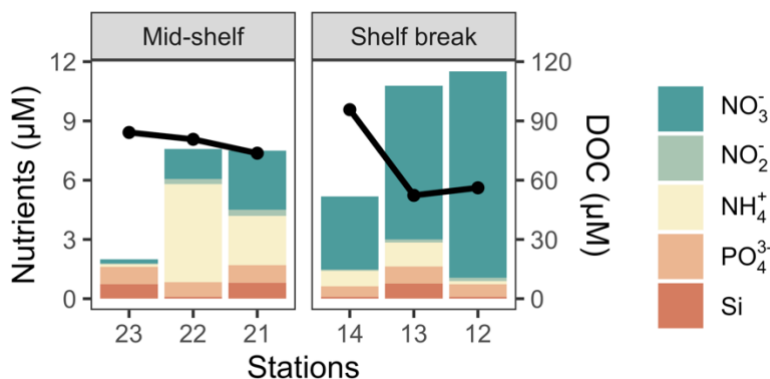
276 **Figure 2. Cumulative nutrient concentrations at the deep chlorophyll-a maximum (bars) and the**

277 **concentration of DOC in surface waters (solid black line) across stations in the mid-shelf and the shelf**

278 **break front.**

279

280
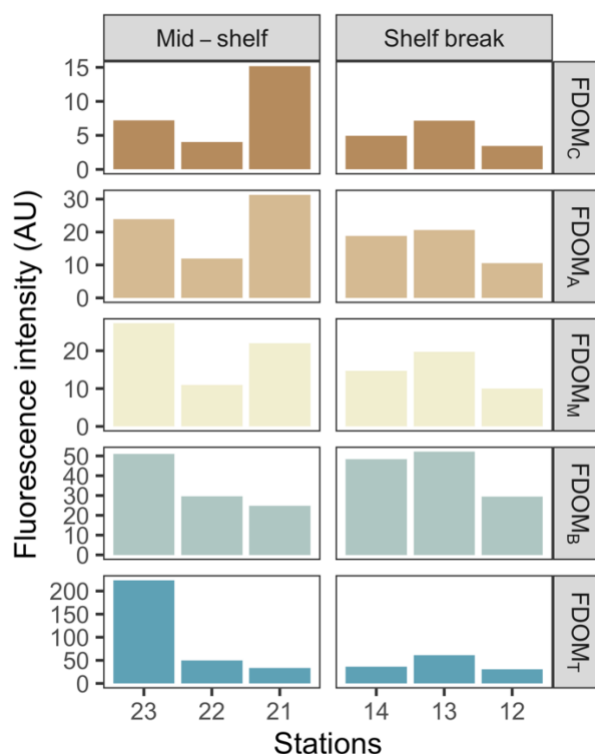
Figure 3. Fluorescence intensity of main identified FDOM components at the deep chlorophyll-a maximum across stations in the mid-shelf and the shelf break front. FDOM components are shown in a decreasing order of humification from top to bottom plots.

284

3.3   Plankton community structure

The biomass of protistan grazers exceeded that of phytoplankton and heterotrophic bacteria at most sampling stations, except at stations 13 and 14, where phytoplankton biomass dominated (Fig. 4a). Heterotrophic dinoflagellates dominated the biomass across stations, except at station 14, where HNP prevailed. In contrast, no clear distribution pattern was observed among phytoplankton groups. Biomass of heterotrophic bacteria ranged between 2.6 (station 22) and 15 µg C L^{-1} (station 14) (Fig. 4b). The abundance of this group was positively associated with chlorophyll-a concentration (R^2=0.7, p=0.04) and the abundance and biomass of most phytoplankton groups (p<0.05), except coccolithophores. The highest bacterial abundance and biomass was registered under chlorophyll-a pulse initiation (stations 21, 13 and 14). Among protistan grazers, the most significant group in terms of biomass were dinoflagellates ranging from 0 (station 14) to 134 µg C L^{-1} (station 22, mostly due to the presence of *Noctiluca scintillans*). Ciliates ranged from 0 (station 14) to 20 µg C L^{-1} (station 21), while HNP showed the highest biomass in stations 13 and 14 (5 and 6 µg C L^{-1}, respectively), and the lowest value was registered in station 12 (0.6 µg C L^{-1}). Plankton <5 µm (choanoflagellates and other unidentified flagellates) was the dominant fraction among HNP except in station 13, were micro-sized ciliates and nano-sized flagellates (*Telonema* sp. and unidentified dinoflagellates) dominated biomass.

300

301
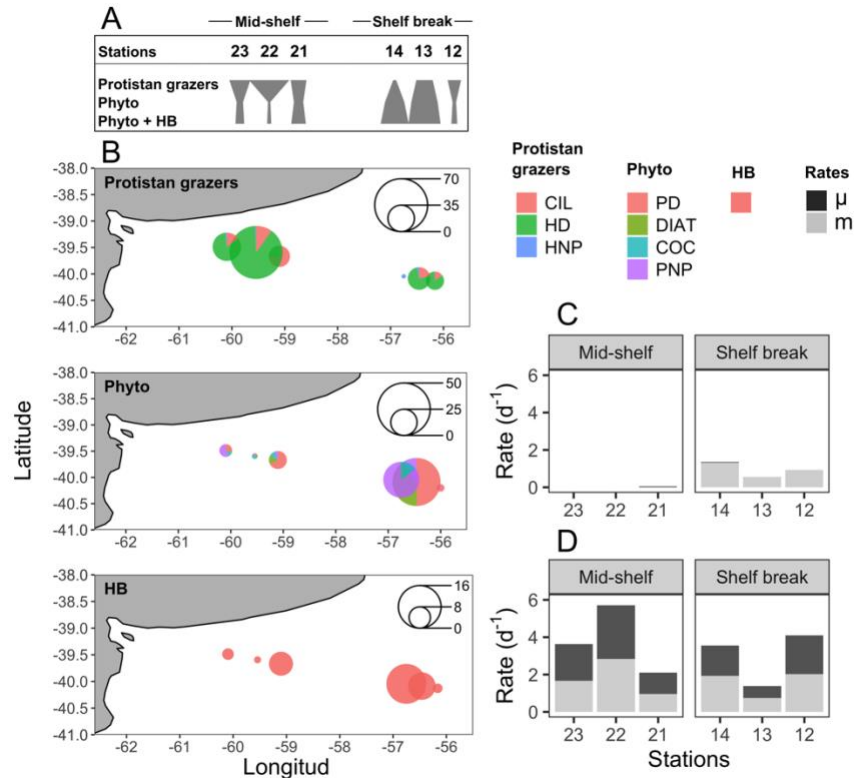
302 **Figure 4.A. Polygons represent the type of food web structure based on the ranking of carbon biomass**

303 **of protistan grazers, phytoplankton (phyto), and heterotrophic bacteria (HB) in each sampling station**

304 **(indicated above the polygons). Inverted or top-heavy pyramids (stations 23, 22, 21 and 12), occur when**

305 **the biomass of protistan grazers surpasses that of their prey (phytoplankton plus HB). In contrast, the**

306 **more conventional bottom-heavy structure (stations 14 and 13), are characterized by a greater prey**

307 **biomass relative to that of consumers. B. Spatial distribution of the cumulative biomass (µg C L^{-1}) of**

308 **protistan grazers (upper plot), phytoplankton (mid-plot) and HB (lower plot). Scale circles are shown**

309 **within each plot. C. Growth (µ) and grazing (m) rates of phytoplankton. D. Growth (µ) and grazing (m)**

310 **rates of HB.**

311

312 The biomass of photosynthetic taxa was generally dominated by PNP. The highest concentration and biomass

313 of all groups, except for coccolithophores, was registered in station 13 (PNF: 32 µg C L^{-1}, PD: 8 µg C L^{-1},

314 diatoms: 6 µg C L^{-1}). High biomass of PNP and dinoflagellates was also registered in station 14 (34 µg C L^{-1})

315 and station 21 (8.5 µg C L^{-1}), respectively. The highest biomass of coccolithophores was registered in station

316 22 (2 µg C L^{-1}).

317 Stations 12 and 13 showed differences on microplankton community structure compared to the rest of the

318 stations (Fig. 5). According to the ordination fit between vectors (i.e., taxa) and stations, the protistan grazers

319 that mainly contributed to separate these two stations from the others were the dinoflagellates *Gymnodinum*

320 spp., and *Protoperidinium pellucidum*, while *Pyramimonas* sp. and *Dinophysis acuminata*, were the distinctive

321 photosynthetic species in these stations (MDS, p<0.05). Stations 22 and 23 were also closely associated

322 regarding the protistan grazers community and the species that contributed most to this association was

323 *Strombidinopsis* sp.

324

325
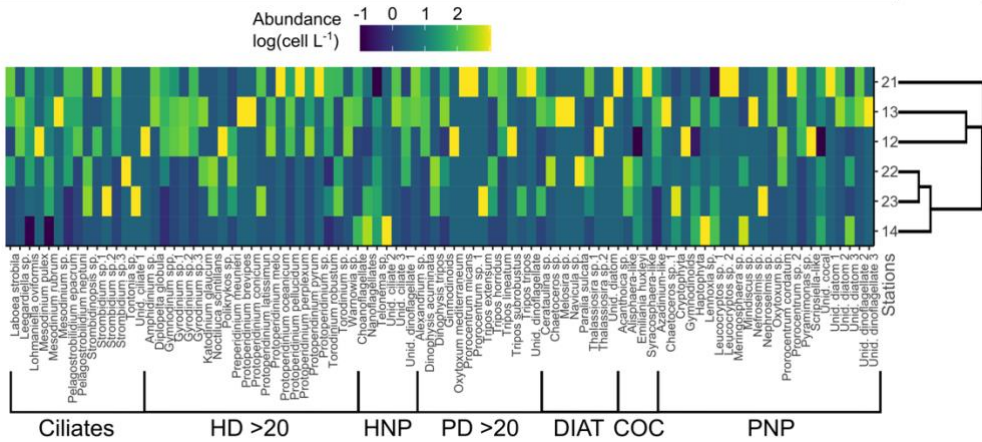
Figure 5. Color-coded, log-transformed cell abundance (cell L⁻¹ × 10³) of plankton taxa (columns) at the sampling stations (rows). Group delimitation is indicated at the bottom. Side dendrogram shows the optimal ordering of rows (stations) so that the sum of distances between each one is minimized. HD>20: Heterotrophic dinoflagellates >20 μm, HNP: Heterotrophic nanoplankton, PD>20: Photosynthetic dinoflagellates >20 μm, Diat: Diatoms, Coc: Coccolithophores, PNP: Photosynthetic nanoplankton.

331

3.4 Growth and grazing rates

333 Water temperature of the incubator container was hourly monitored and ranged between 12.2 and 13.8°C in the mid-shelf stations and between 8 and 11.1°C in the shelf break stations. Bacteria showed active growth during all experiments while phytoplankton only revealed significant growth rates in conditions of pulse initiation (stations 21 and 14). Some degree of nutrient limitation was detected in the mid-shelf stations as the growth rate of phytoplankton at the control treatments was lower than in the nutrient amended treatment, however, differences were not statistically significant. No apparent differences were found in stations 12, 13 and 14. Significant grazing effect on bacteria was found in all experiments (Fig. 4c), while grazing on phytoplankton was only significant in the shelf break stations (Fig. 4d). In the mid-shelf stations, daily bacterial productivity consumed by HNP averaged 72%, while in the shelf break stations, it reached 83%. Mean daily primary productivity consumed by protistan grazers was zero in the mid-shelf stations and 155% in the shelf break. Linear responses were found in all experiments, indicating that no cascading effects, saturating feeding or starvation occurred within incubation bottles. The abundance of heterotrophic bacteria was negatively correlated with the grazing of HNP (R^2=0.8, p=0.016) and growth (R^2=0.9, p=0.005).

346

3.5 Short-term DOM transformations

348 An accumulation of the a254 DOM fraction was observed in stations 22, 14, 13, and 12 during the incubation period in the experimental setting with protists, while stations 23 and 21 exhibited DOM consumption (Fig. 6a).

350 Conversely, in the experimental setting without protists, the a254 DOM fraction accumulated in stations 22, 21,
351 14, and 12, while stations 23 and 13 showed DOM consumption (Fig. 7a). Regardless of net DOM production,
352 biodegradation of organic matter occurred in most experiments as denoted by the decrease in the BIX and the
353 increase in the HIX (Fig. 6b, 7b). The prevalence of biodegradation over UV photodegradation or adsorption
354 was further supported by most source discrimination indices (FI and M/A, data not shown). The decrease in
355 BIX was coherent with the net zero to low phytoplankton growth during our experiments. An exception to this
356 general pattern occurred in station 13, in which HIX increased and BIX decreased during the incubation. Station
357 13 was characterized by the highest abundance of micro-sized phytoplankton (diatoms and photosynthetic
358 dinoflagellates) and registered the lowest concentration of DOC (52 µM) at the moment of sampling. While
359 HIX and BIX indices suggested that DOM modifications are not driven by biodegradation, M/A decreased and
360 FI increased during the experiments, thus giving inconsistent results.
361 Among treatments, a shift from accumulation to consumption of the a254 DOM fraction was registered in
362 stations 21 and 13. In the presence of protists, the net a254 fraction of DOM change was negatively associated
363 with the fluorescence intensity of peaks related to humic-like compounds (FDOM$_C$: R^2=0.6, p=0.07, FDOM$_A$,
364 R^2=0.8, p=0.01, FDOM$_M$: R^2=0.7, p=0.04), and positively associated with the grazing on HB (R^2=0.7, p=0.00,
365 Fig. 8a). In the absence of protists, the net a254 fraction of DOM change was negatively associated with the
366 ratio between bacteria and phytoplankton biomass (R^2=0.9, p=0.01, Fig. 8b).
367
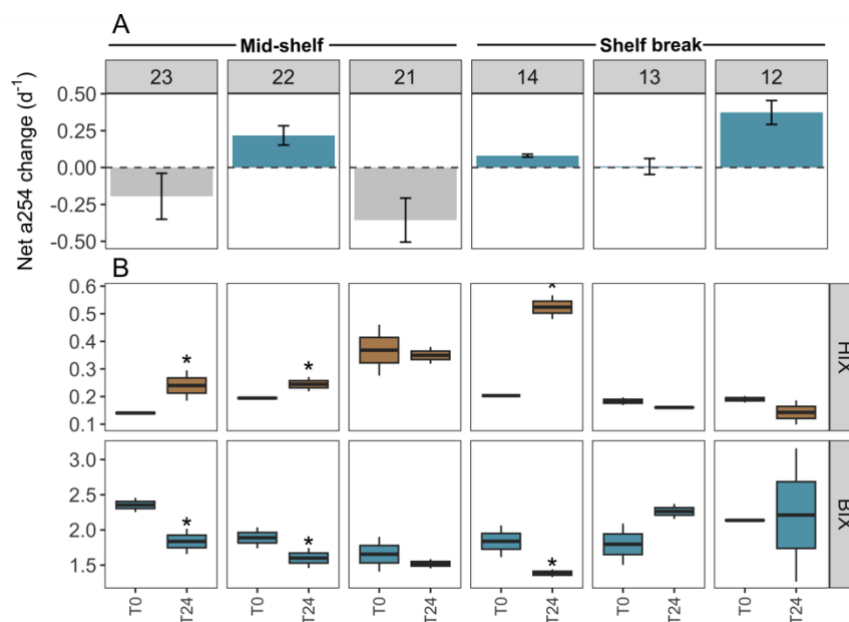
368
369 **Figure 6. DOM transformations in the experimental setting with protists (pre-filtered by 200 µm) across**
370 **stations in the mid-shelf and the shelf break front. A. Net changes in the absorbance at 254 nm (a254)**
371 **from the chromophoric fraction of DOM, a proxy of total DOM concentration. Dashed line indicates the**
372 **limit between negative (i.e., consumption) and positive net a254 changes (i.e., accumulation) during the**
373 **incubation period. B. Shifts in the humification index (HIX) and the biological activity index (BIX) during**

376

377

378   **Figure 7. DOM transformations in the experimental setting without protists (pre-filtered by 0.7 µm)**

379   **across stations in the mid-shelf and the shelf break front. A. Net changes in the absorbance at 254 nm**

380   **(a254) from the chromophoric fraction of DOM, a proxy of total DOM concentration. Dashed line**

381   **indicates the limit between negative (i.e., consumption) and positive net a254 changes (i.e., accumulation)**

382   **during the incubation period. B. Shift in the humification index (HIX) and the biological activity index**

383   **(BIX) during the 24-h incubation. Asterisks indicate significant differences identified by linear regression**

384   **analysis between initial and final treatments (p<0.05).**

385
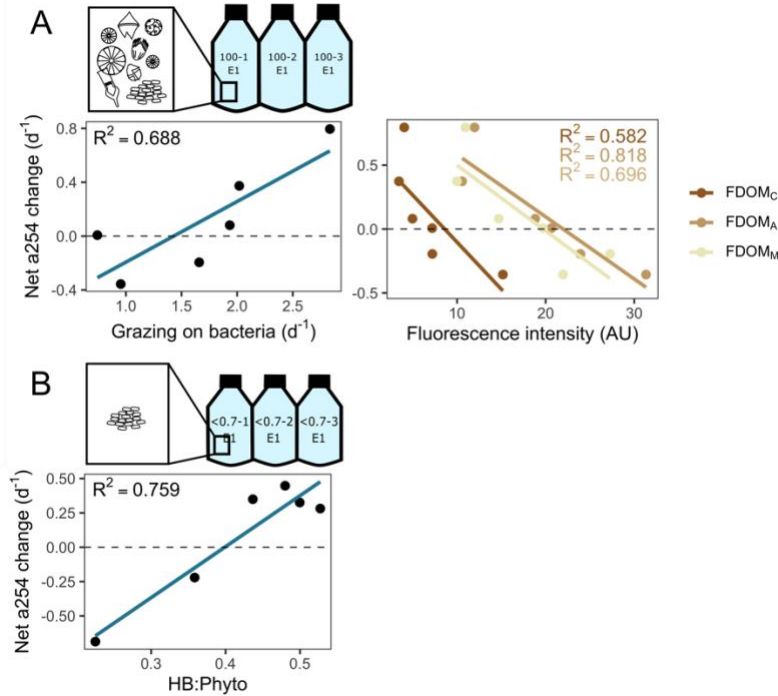
Figure 8. Main predictors of the net changes in the absorbance at 254 nm (a254) from the chromophoric fraction of DOM during incubations. A. Experimental setting with protists. Linear regression plots depict the relationship between net a254 changes and grazing on bacteria, and humic-like substances (as depicted by fluorophores FDOM$_C$, FDOM$_A$, and FDOM$_M$). B. Experimental setting without protists. Linear regression plot depicts the relationship between net a245 changes and the ratio between heterotrophic bacteria (HB) and phytoplankton (Phyto) biomass. Dashed lines indicate the limit between negative (i.e., consumption) and positive (i.e., accumulation) net a254 changes.

4   Discussion

4.1   Microbial food web structure

Plankton composition and distribution varied notably across blooming and non-blooming stations, with station 14 standing out for its atypical plankton structure within a bloom region. Dominated by a nanoplanktonic diatom and a small grazer community, this station also showed high bacterial biomass, likely due to low PO_4^{3-} and Si concentrations, but high DOC levels. Nanoplankton, particularly diatoms, cryptophytes, and haptophytes, were predominant across sampling stations, with cyanobacteria assumed to play a significant role in carbon fixation. Similar findings were reported in previous studies by Silva et al. (2009) and Negri et al. (2013; 2016), indicating the widespread dominance of plankton <5 µm in the region.

In the shelf break front, dinoflagellates dominated both photosynthetic and heterotrophic biomass, while ciliates were more abundant in the mid-shelf. Besides these spatial differences, the lack of a clear distribution pattern of plankton highlights the impact of mesoscale structures on spatial plankton heterogeneity (Lehahn et al., 2018), a feature proper of the Patagonian Shelf (Saraceno et al., 2024). Heterotrophic bacterial abundance was comparable to coastal summer values reported by Hozbor et al. (2013), Negri et al. (2016), and Garzón-Cardona

409 et al. (2021). It exhibited a positive correlation with chlorophyll-a, but was negatively affected by HNP grazing.
410 This dynamic suggests that bacterial populations are primarily regulated by grazing pressure and the availability
411 of phytoplankton-derived DOM, rather than by nutrient limitation during periods of high productivity.
412

4.2 Microbial trophic pathways

414 In oligotrophic areas, microbial food webs involve multi-step carbon transfer dominated by small organisms
415 that efficiently recycle nutrients. By contrast, productive regions have shorter, more efficient food webs where
416 carbon moves directly to higher trophic levels (Armengol et al., 2019). Our observations showed strong
417 microbial trophic coupling across the mid-shelf and the shelf break front, however under more productive
418 conditions, a fraction of primary producers escaped grazing. Mid-shelf stations, including post-bloom station
419 12, exhibited an "inverted pyramid" biomass structure, where consumer biomass exceeded that of their prey
420 suggesting high trophic efficiency, as shown in former studies (McCauley et al., 2018). In the shelf break front,
421 despite evidence of protistan herbivory, much of the phytoplankton biomass remained ungrazed likely due to
422 strong top-down pressure from microcrustaceans on both phytoplankton and protistan grazers. This created a
423 more typical bottom-heavy biomass structure, indicative of high primary productivity where some primary
424 production bypasses protist predation and is consumed by microcrustaceans or exported. Such a food web
425 configuration achieves the highest carbon biomass, regardless of community composition (Kang et al., 2023).
426 These observations align with previous findings in the shelf region, showing strong trophic coupling and
427 minimal sinking of unused biomass, dominated by small phytoplankton (<5 µm) and balanced biomass levels
428 of micro- and mesozooplankton (Negri et al., 2013).
429 Our findings showed active growth of heterotrophic bacteria across all stations, while phytoplankton exhibited
430 low net growth or biomass yield, except at two stations undergoing developing bloom stages (14 and 21).
431 Heterotrophic bacteria, despite having half the biomass of phytoplankton, was selectively preyed by protistan
432 grazers, accounting for 72% of bacterial production in mid-shelf stations and 83% in the shelf break front (Fig.
433 9). This preference for bacteria likely stems from their higher growth rate compared to phytoplankton, as
434 protistan grazing is primarily triggered by prey growth rate rather than biomass (Banse, 1982; Calbet and
435 Landry, 2004; Chen et al., 2009). Regarding the low phytoplankton growth rates observed in this study, an
436 additional factor beyond bloom timing may involve UV photoinhibition, which can affect some eukaryotic
437 pigmented plankton when exposed to deck conditions. Although light conditions were carefully controlled
438 during handling and the incubator was covered with a special net to prevent overexposure, continuous light
439 exposure cannot fully replicate the natural mitigation of UV stress provided by vertical mixing in the water
440 column (Häder et al., 2015). Laws et al. (2000) noted unrealistic growth estimates, attributing the negative
441 effects of UV exposure to phytoplankton incubation at the surface. Simulating natural UV exposure remains a
442 common challenge in most incubation experiments, where communities experience more stable light
443 conditions.
444 Our results showed that bacteria exhibited growth advantages over phytoplankton across the examined
445 environmental gradient but were concurrently more vulnerable to grazing pressure. This compensatory grazing
446 on fast-growing bacteria has been previously observed in productive environments such as the California

447 Current (Goericke, 2011; Taylor and Landry, 2018; Landry et al., 2023), as well as in the oligotrophic Warm

448 Taiwan Current (Chiang et al., 2014). The suggested mechanism underlying this trophic interaction posits that

449 increased phytoplankton-DOM production fosters the growth of resource-efficient bacteria, as suggested by the

450 tight coupling between bacteria and phytoplankton biomass. However, the heightened growth, coupled with a

451 diminished allocation of energy to defensive skills, renders these bacteria susceptible to selective grazing

452 (Taylor and Landry, 2018).

453 The situation in the more productive shelf break front shifted toward a coupled predation upon both prokaryotes

454 and phytoplankton (Fig. 9). Grazing accounted for 83% of bacterial production and 154% of phytoplankton

455 production. Despite limited growth, phytoplankton faced substantial grazing pressure, possibly facilitated by

456 shared predators with bacteria. This trophic interaction aligns with the enhanced microbial loop hypothesis

457 (Taylor and Landry, 2018), suggesting that small phytoplankton is increasingly grazed as a byproduct of grazers

458 actively preying on bacteria under conditions of rising productivity. Under this scenario, grazing on

459 picophytoplankton is density-independent and occurs due to the presence of shared common grazers with

460 bacteria. Overall, bacteria appeared to be positively regulated by commensalism with phytoplankton and

461 negatively by grazing, constituting a primary carbon source for protistan grazers regardless of the productivity

462 level.

463 An additional factor contributing to grazing selectivity across productivity areas may be related to grazer

464 community composition, which differed between the mid-shelf and the shelf break front, with ciliates more

465 concentrated on the mid-shelf and heterotrophic dinoflagellates more associated with shelf break stations

466 (especially in stations 12 and 13). In contrast, phytoplankton structure showed no distinct regional differences.

467 Ciliates primarily select prey based on size due to their oral diameter, while dinoflagellates employ diverse

468 feeding strategies, allowing them access to a broader range of prey sizes. This trait positions dinoflagellates as

469 key grazers in meso- and eutrophic environments, such as upwelling areas (e.g., Hansen et al., 1997; Sherr and

470 Sherr, 2007; Calbet, 2008), enabling them to effectively target both bacteria and larger phytoplankton.

471

472 **4.3   Short-term DOM pathways**

473 Throughout the experiments, substantial bacterial proliferation and minimal or no phytoplankton growth were

474 observed to occur alongside the active biodegradation of organic matter, as evidenced by a decrease in the

475 biological index (BIX) and an increase in the humification index (HIX). The general decreasing trend of BIX

476 during the incubation and its similar behaviour in the absence of protist confirms a bacterial effect and suggests

477 that bacteria are rapidly consuming recently produced phytoplankton exudates. Comparable observations have

478 shown that bacteria produce humic-like substances from protistan plankton precursors in controlled

479 environments absent of terrestrial influence (Gruber et al., 2006; Romera-Castillo et al., 2011; Lechtenfeld et

480 al., 2015; Kinsey et al., 2018; Osburn et al., 2019), underscoring the pivotal role of microbial communities in

481 converting DOM into refractory substances over brief timescales. The described carbon route partially explains

482 why the region acts as a carbon sink throughout most of the year (Kahl et al., 2017), irrespective of the

483 magnitude of primary productivity, and emphasize the critical role of the microbial carbon pump (Jiao et al.,

484 2010) as a key carbon sequestration pathway on the northern Patagonian Shelf. While these findings highlight

485 its importance, the seasonal relevance of this mechanism remains to be explored.

486 The accumulation of a fraction of DOM, as indicated by a254, was not limited to stations experiencing active

487 phytoplankton growth, indicating that net DOM release is not necessarily tied to specific phenological stages,

488 as previously suggested (Bachi et al., 2023). Moreover, accumulation occurred under diverse phytoplankton

489 assemblages, implying a low level of specialization in the bacterial utilization of species-specific DOM

490 substances, a trait that becomes apparent under conditions of high resource availability (Sarmento et al., 2016).

491 The complexity of DOM, reflected by the prevalence of humic-like compounds ($FDOM_C$, $FDOM_A$, and

492 $FDOM_M$), emerged as a key factor influencing its bacterial utilization. A net consumption of the DOM fraction,

493 as estimated by a254, was observed when the initial pool contained a significant proportion of low-reactivity

494 compounds, influenced by the phenological status of the sampling site, as indicated by satellite chlorophyll-a

495 trends. At stations 23 and 21, low prior chlorophyll-a indicated limited recent autochthonous DOM production.

496 However, bacterial activity differed between the two stations. At station 23, elevated bacterial activity resulted

497 in a notable increase in DOM complexity and net consumption under both treatments, indicating that bacteria

498 depended on a substantial initial labile DOM pool ($FDOM_T$), despite the predominance of refractory

499 compounds. In contrast, station 21 exhibited low bacterial activity, with the a254 DOM fraction shifting from

500 consumption to accumulation in the absence of protists. This indicated bacterial reliance on phytoplankton

501 DOM exudates when the DOM pool is primarily refractory.

502 At station 13, the opposite pattern was observed, with the a254 DOM fraction shifting from weak accumulation

503 in the presence of protists, to consumption in the absence of protists. Here, a higher proportion of labile DOM

504 facilitated bacterial activity. Low phytoplankton-to-bacteria biomass ratios indicated that bacterial DOM

505 consumption was masked by phytoplankton biomass but became evident without protists. However, DOM

506 accumulation may also reflect viral lysis, as suggested by HIX decreases and BIX increases, alongside low

507 bacterial growth and grazing. Overall, the initial proportion of refractory compounds better predicted the net

508 DOM production by providing insights on microbial succession trajectories.

509
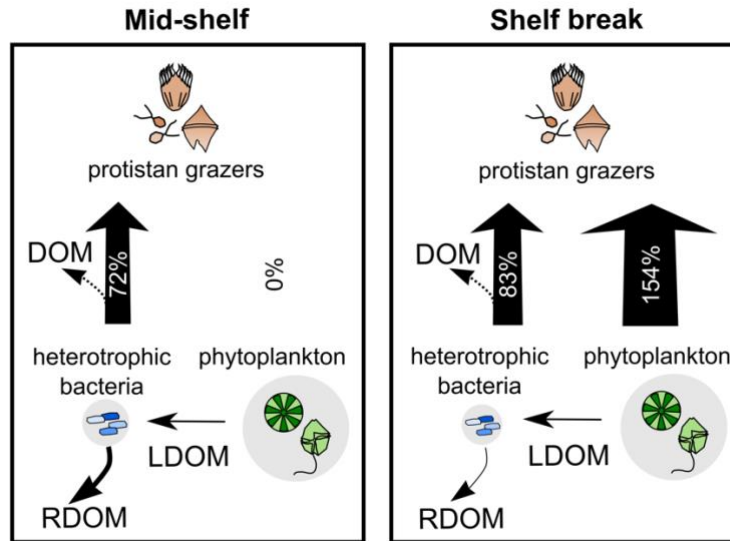
Figure 9. Schematic representation of DOM pathways during the productive season on the Patagonian Shelf, contrasting the mid-shelf (low-to-moderate productivity, left panel) with the shelf break front (high productivity, right panel). Phytoplankton biomass (background circle size) was twice that of bacteria, with selective grazing on bacteria balancing their rapid growth across sampling areas. Grazing on phytoplankton increased under higher productivity, aligning with the enhanced microbial loop hypothesis. Heterotrophic bacteria were key in shaping DOM quality, utilizing labile DOM (LDOM) from phytoplankton and contributing to the storage of refractory DOM (RDOM), even without DOM-producing protists. RDOM production was more pronounced mid-shelf than at the shelf break. Bacterial grazing influenced the net production of the a254 DOM fraction, with intense grazing leading to DOM accumulation likely through reduced bacterial biomass and egested organic material. Arrow thickness represents grazing pressure, with percentages indicating daily grazed productivity.

The a254 DOM fraction also tended to accumulate under high bacterial mortality due to grazing. Our results evidenced a selective grazing on bacteria compensating for their fast growth rate. This group-specific grazing mortality aligns well with the grazing selectivity model, wherein grazers exhibit preferences against high-growth-rate organisms, establishing a tight coupling between growth advantages and grazing vulnerability across environmental gradients (Landry et al., 2023). Our experimental data not only support this hypothesis but also provide new insights into the repercussions of bacterial grazing on dissolved carbon stocks (Fig. 9). Specifically, our results suggest that grazing on bacteria can lead to an accumulation of DOM produced by phytoplankton by reducing the biomass of bacterial standing stock. In addition, protistan grazing may contribute to the DOM pool by releasing bacterial carbon (Taylor et al., 1985). However, bacteria may not immediately utilize this DOM source, as adapting their enzymatic machinery to target new compounds requires additional energy expenditure, resulting in less efficient resource utilization (Baña et al., 2014). Similar results were observed in polar waters, where high protistan bacterivory was associated with DOM accumulation (Lund Paulsen et al., 2019). Our observations carry biogeochemical implications, as intense bacterial grazing implies

536 that bacterial biomass becomes available to higher trophic levels, thereby circumventing the DOM cycle. In
537 other words, while most bacterial biomass is directed by protistan grazers toward higher trophic levels, it also
538 partially diverts the production of DOM lysates by viral lysis (Suttle, 2005). Our experimental results also
539 indicate that intense grazing only partially compensates for this carbon route, as protistan grazing contributes
540 with additional DOM substances while a fraction of phytoplankton-derived DOM remains unexploited by
541 bacteria over short timescales.

542 Protistan grazing is widely recognized as the primary driver of phytoplankton mortality (Calbet and Landry,
543 2004) and is an important mortality source for heterotrophic bacteria (Weinbauer and Peduzzi, 1995). However,
544 viral lysis can achieve comparable mortality rates in both phytoplankton and bacterial populations to that caused
545 by protistan grazers. Discerning the viral impact within incubation bottles can be challenging, as viral activity
546 may not only contribute to cell lysis but has been observed to stimulate prey availability for protists, potentially
547 through the release of cellular lysates or by reducing competition (Staniewski and Short, 2014). In our study,
548 while protist grazing was considered the primary cause of bacterial and phytoplankton mortality, we
549 acknowledge that viral lysis may have also played an unrecognized but significant role in the dilution
550 experiments.

551 The fate of grazing-derived DOM remains uncertain in our experimental setup, as it could either serve as a
552 potential source for bacterial utilization, thus establishing positive longer-term predator-prey feedback not
553 captured in our 24-h experiment, or contribute to the complex DOM pool, feeding into the refractory fraction.
554 Indeed, previous observations revealed that DOM derived from protistan grazers varies in its bioavailability
555 (Taylor et al., 1985), and their complexity is further shaped by taxa composition (Nagata and Kirchman, 1992;
556 Gruber et al., 2006). In our experiments, we did not observe a clear trend in DOM transformation between
557 treatments with and without protists, indicating that bacteria remain as the primary drivers of DOM quality.
558 Overall, our finding revealed that under high bacterial growth rate that follows the onset of the productive
559 season, protistan grazers not only channels carbon through remineralization but also, foster the degree of DOM
560 accumulation by reducing DOM-degrading bacterial stock and/or contributing with egestion substances.
561 Additionally, instead of acting solely as a sink of carbon through mineralization of organic compounds, bacteria
562 serve as a crucial link between assimilatory CO_2 and higher trophic levels.
563

564 **Data availability**
565 DOI: 10.5281/zenodo.11662261
566

567 **Authors contribution**
568 CLA conceptualized, designed, and carried out the experiments, analyzed plankton samples and acquired
569 funding. JEGC, AM and ASG analyzed DOC, optical properties of DOM and nutrients samples and interpreted
570 the results. JEGC performed the PARAFAC multivariate algorithm and calculated fluorescence indices. RS
571 analyzed plankton samples and performed biomass calculations. JCM contributed to the numerical
572 methodology design and the conceptualization of overarching goals. LARE analyzed and interpreted CTD data

573 and Moderate Resolution Imaging Spectroradiometer (MODIS) Aqua images of chlorophyll-a. RL coordinated
574 responsibilities for the research activities planning and execution, acquired funding and contributed to the
575 conceptualization of overarching goals. CLA prepared the manuscript with contributions from all co-authors.
576

Competing interests

578 The authors declare no competing interests.
579

Acknowledgments

581 We are thankful to the crew of the RV "Dr. Bernardo Houssay" of Prefectura Naval Argentina for their support
582 on field activities and sampling. This study was supported by the National Agency for Promotion of Science
583 and Technology (FONCYT-PICT 0467–2010 and FONCYT-PICT 2386-2017), the National Scientific and
584 Technical Research Council (CONICET-PIP 11220200102681CO) and by the Argentine Oceanographic
585 Institute (IADO, CONICET-UNS). The authors acknowledge that language checking and spelling
586 improvements were done by ChatGPT (powered by OpenAI's language model, GPT-3; http://openai.com).
587

References

589 Armengol, L., Calbet, A., Franchy, G., Rodríguez-Santos, A., and Hernández-León, S.: Planktonic food web
590   structure and trophic transfer efficiency along a productivity gradient in the tropical and subtropical
591   Atlantic Ocean. Sci Rep, 9, 2044, https://doi.org/10.1038/s41598-019-38507-9, 2019.

592 Bachi, G., Morelli, E., Gonnelli, M., Balestra, C., Casotti, R., Evangelista, V., Repeta, D. J., and Santinelli, C.:
593   Fluorescent properties of marine phytoplankton exudates and lability to marine heterotrophic
594   prokaryotes degradation, Limnol Oceanogr, 68, https://doi.org/10.1002/lno.12325, 2023.

595 Bai, Y., Su, R., Han, X., Zhang, C., and Shi, X.: Investigation of seasonal variability of CDOM fluorescence in
596   the southern changjiang river estuary by EEM-PARAFAC, Acta Oceanologica Sinica, 34, 1–12,
597   https://doi.org/10.1007/s13131-015-0714-8, 2015.

598 Baltar, F., Palovaara, J., Unrein, F., Catala, P., Horňák, K., Šimek, K., Vaqué, D., Massana, R., Gasol, J. M.,
599   and Pinhassi, J.: Marine bacterial community structure resilience to changes in protist predation under
600   phytoplankton bloom conditions, ISME J, 10, 568–581, https://doi.org/10.1038/ismej.2015.135, 2016.

601 Baña, Z., Ayo, B., Marrasé, C., Gasol, J. M., and Iriberri, J.: Changes in bacterial metabolism as a response to
602   dissolved organic matter modification during protozoan grazing in coastal Cantabrian and
603   Mediterranean waters, Environ Microbiol, 16, 498–511, https://doi.org/10.1111/1462-2920.12274,
604   2014.

605 Banse, K.: Cell volumes, maximal growth rates of unicellular algae and ciliates, and the role of ciliates in the
606   marine pelagial, Limnol Oceanogr, 27, 1059–1071, https://doi.org/10.4319/lo.1982.27.6.1059, 1982.

607 Berden, G., Charo, M., Möller, O. O., and Piola, A. R.: Circulation and Hydrography in the Western South
608   Atlantic Shelf and Export to the Deep Adjacent Ocean: 30°S to 40°S, J Geophys Res Oceans, 125,
609   https://doi.org/10.1029/2020JC016500, 2020.

610 Berglund, J., Müren, U., Båmstedt, U., and Andersson, A.: Efficiency of a phytoplankton-based and a bacterial-
611   based food web in a pelagic marine system, Limnol Oceanogr, 52, 121–131,
612   https://doi.org/10.4319/lo.2007.52.1.0121, 2007.

613 Brandstetter, A., Sletten, R. S., Mentler, A., and Wenzel, W. W.: Estimating dissolved organic carbon in natural
614   waters by UV absorbance (254 nm), Zeitschrift für Pflanzenernährung und Bodenkunde, 159, 605–
615   607, https://doi.org/10.1002/jpln.1996.3581590612, 1996.

616 Calbet, A.: The trophic roles of microzooplankton in marine systems. ICES J, 65, 325-331,
617   https://doi.org/10.1093/icesjms/fsn013, 2008.

618 Calbet, A. and Landry, M. R.: Phytoplankton growth, microzooplankton grazing, and carbon cycling in marine
619   systems, Limnol Oceanogr Methods, 49, 51–57, https://doi.org/10.4319/lo.2004.49.1.0051, 2004.

620 Calbet, A. and Saiz, E.: How much is enough for nutrients in microzooplankton dilution grazing experiments?,
621   J Plankton Res, 40, 109–117, https://doi.org/10.1093/plankt/fbx070, 2018.

622 Chen, B., Liu, H., Landry, M. R., DaI, M., Huang, B., and Sune, J.: Close coupling between phytoplankton
623   growth and microzooplankton grazing in the western South China Sea, Limnol Oceanogr, 54, 1084–
624   1097, https://doi.org/10.4319/lo.2009.54.4.1084, 2009.

625 Chiang, K.-P., Tsai, A.-Y., Tsai, P.-J., Gong, G.-C., Huang, B.-Q., and Tsai, S.-F.: The influence of
626   nanoflagellates on the spatial variety of picoplankton and the carbon flow of the microbial food web
627   in the oligotrophic subtropical pelagic continental shelf ecosystem, Cont Shelf Res, 80, 57–66,
628   https://doi.org/10.1016/j.csr.2014.02.019, 2014.

629 Coble, P. G.: Characterization of marine and terrestrial DOM in seawater using excitation-emission matrix
630   spectroscopy, Mar Chem, 51, 325–346, https://doi.org/10.1016/0304-4203(95)00062-3, 1996.

631 Delgado, A. L., Hernández-Carrasco, I., Combes, V., Font-Muñoz, J., Pratolongo, P. D., and Basterretxea, G.:
632   Patterns and Trends in Chlorophyll-a Concentration and Phytoplankton Phenology in the
633   Biogeographical Regions of Southwestern Atlantic, J Geophys Res Oceans, 128,
634   https://doi.org/10.1029/2023JC019865, 2023.

635 Drozdova, A. N., Krylov, I. N., Nedospasov, A. A., Arashkevich, E. G., and Labutin, T. A.: Fluorescent
636   signatures of autochthonous dissolved organic matter production in Siberian shelf seas. Front Mar Sci
637   9:872557. https://doi:10.3389/fmars.2022.872557, 2022.

638 Ferronato, C., Berden, G., Rivarossa, M., and Guinder, V. A.: Wind-driven currents and water masses shape
639   spring phytoplankton distribution and composition in hydrologically complex, productive shelf waters,
640   Limnol Oceanogr, 68, 2195–2210, https://doi.org/10.1002/lno.12413, 2023.

641 Garzón-Cardona, J. E., Guinder, V. A., Alonso, C., Martínez, A. M., Pantoja-Gutiérrez, S., Kopprio, G. A.,
642   Krock, B., and Lara, R. J.: Chemically unidentified dissolved organic carbon: A pivotal piece for
643   microbial activity in a productive area of the Northern Patagonian shelf, Mar Environ Res, 167,
644   105286, https://doi.org/10.1016/j.marenvres.2021.105286, 2021.

645 Goericke, R.: The structure of marine phytoplankton communities-patterns, rules and mechanisms, California
646   Cooperative Oceanic Fisheries Investigation Reports, 52, 182–197, 2011.

647 Gruber, D. F., Simjouw, J.-P., Seitzinger, S. P., and Taghon, G. L.: Dynamics and characterization of refractory
648   dissolved organic matter produced by a pure bacterial culture in an experimental predator-prey system,
649   Appl Environ Microbiol, 72, 4184–4191, https://doi.org/10.1128/AEM.02882-05, 2006.

650 Hach, P. F., Marchant, H. K., Krupke, A., Riedel, T., Meier, D. V., Lavik, G., Holtappels, M., Dittmar, T., and
651   Kuypers, M. M. M.: Rapid microbial diversification of dissolved organic matter in oceanic surface
652   waters leads to carbon sequestration, Sci Rep, 10, 13025, https://doi.org/10.1038/s41598-020-69930-
653   y, 2020.

654 Häder, D. P., Williamson, C. E., Wängberg, S. Å., Rautio, M., Rose, K. C., Gao, K., Helbling, W. E., Sinha, R.
655   P., and Worrest, R.: Effects of UV radiation on aquatic ecosystems and interactions with other
656   environmental factors. Photochem Photobiol Sci, 14(1), 108-126, https://doi:10.1039/c4pp90035a,
657   2015.

658 Hansen, P. J., Bjørnsen, P. K., and Hansen, B. W.: Zooplankton grazing and growth: Scaling within the 2-2,000-
659   µm body size range. Limnol Oceanogr, 42, 687-704, https://doi.org/10.4319/lo.1997.42.4.0687, 1997.

660 Hillebrand, H., Dürselen, C., Kirschtel, D., Pollingher, U., and Zohary, T.: Biovolume calculation for pelagic
661   and benthic microalgae, J Phycol, 35, 403–424, https://doi.org/10.1046/j.1529-8817.1999.3520403.x,
662   1999.

663 Hozbor, M. C., Hernández, D. R., Cucchi Colleoni, A. D., Costagliola, M. C., and Peressutti, S. R.: Biomasa y
664   distribución espacial del bacterioplancton en el sector norte de la plataforma continental argentina (34º
665   S-41º S), Revista de Investigación y Desarrollo Pesquero, 23, 145–160, 2013.

666 Huguet, A., Vacher, L., Relexans, S., Saubusse, S., Froidefond, J. M., and Parlanti, E.: Properties of fluorescent
667   dissolved organic matter in the Gironde Estuary, Org Geochem, 40, 706–719,
668   https://doi.org/10.1016/j.orggeochem.2009.03.002, 2009.

669 Hutchins, D. A. and Fu, F.: Microorganisms and ocean global change, Nat Microbiol, 2, 17058,
670   https://doi.org/10.1038/nmicrobiol.2017.58, 2017.

671 Irigoien, X., Flynn, K. J., and Harris, R. P.: Phytoplankton blooms: a 'loophole' in microzooplankton grazing
672   impact?, J Plankton Res, 27, 313–321, https://doi.org/10.1093/plankt/fbi011, 2005.

673 Jeffrey, S. W. and Humphrey, G. F.: New spectrophotometric equations for determining chlorophylls a, b, c1
674   and c2 in higher plants, algae and natural phytoplankton, Biochemie und Physiologie der Pflanzen,
675   167, 191–194, https://doi.org/10.1016/S0015-3796(17)30778-3, 1975.

676 Jiao, N., Herndl, G. J., Hansell, D. A., Benner, R., Kattner, G., Wilhelm, S. W., Kirchman, D. L., Weinbauer,
677   M. G., Luo, T., Chen, F., and Azam, F.: Microbial production of recalcitrant dissolved organic matter:
678   long-term carbon storage in the global ocean. Nat Rev Microbiol, 8, 593–599,
679   https://doi.org/10.1038/nrmicro2386, 2010.

680 Jørgensen, L., Stedmon, C. A., Kragh, T., Markager, S., Middelboe, M., and Søndergaard, M.: Global trends in
681   the fluorescence characteristics and distribution of marine dissolved organic matter. Mar Chem, 126(1–
682   4), 139–148, https://doi.org/10.1016/j.marchem.2011.05.002, 2011.

Kahl, L. C., Bianchi, A. A., Osiroff, A. P., Pino, D. R., and Piola, A. R.: Distribution of sea-air CO2 fluxes in the Patagonian Sea: Seasonal, biological and thermal effects, Cont Shelf Res, 143, 18–28, https://doi.org/10.1016/j.csr.2017.05.011, 2017.

Kanayama, T., Kobari, T., Suzuki, K., Yoshie, N., Honma, T., Karu, F., and Kume, G.: Impact of microzooplankton grazing on the phytoplankton community in the Kuroshio of the East China sea: A major trophic pathway of the Kuroshio ecosystem, Deep-Sea Res I: Oceanogr Res Pap, 163, 103337, https://doi.org/10.1016/j.dsr.2020.103337, 2020.

Kang, H. C., Jeong, H. J., Ok, J. H., Lim, A. S., Lee, K., You, J. H., Park, S. A., Eom, S. H., Lee, S. Y., Lee, K. H., Jang, S. H., Yoo, Y. Du, Lee, M. J., and Kim, K. Y.: Food web structure for high carbon retention in marine plankton communities, Sci Adv, 9, https://doi.org/10.1126/sciadv.adk0842, 2023.

Kattner, G. and Becker, H.: Nutrients and organic nitrogenous compounds in the marginal ice zone of the Fram Strait, J Mar Syst, 2, 385–394, https://doi.org/10.1016/0924-7963(91)90043-T, 1991.

Kinsey, J. D., Corradino, G., Ziervogel, K., Schnetzer, A., and Osburn, C. L.: Formation of chromophoric dissolved organic matter by bacterial degradation of phytoplankton-derived aggregates, Front Mar Sci, 4, https://doi.org/10.3389/fmars.2017.00430, 2018.

Kujawinski, E. B., Del Vecchio, R., Blough, N. V., Klein, G. C., and Marshall, A. G.: Probing molecular-level transformations of dissolved organic matter: insights on photochemical degradation and protozoan modification of DOM from electrospray ionization Fourier transform ion cyclotron resonance mass spectrometry, Mar Chem, 92, 23–37, https://doi.org/10.1016/j.marchem.2004.06.038, 2004.

Landry, M. R. and Hassett, R. P.: Estimating the grazing impact of marine micro-zooplankton, Mar Biol, 67, 283–288, https://doi.org/10.1007/BF00397668, 1982.

Landry, M. R., Stukel, M. R., Selph, K. E., and Goericke, R.: Coexisting picoplankton experience different relative grazing pressures across an ocean productivity gradient, Proc Natl Acad Sci USA, 120, https://doi.org/10.1073/pnas.2220771120, 2023.

Laruelle, G. G., Cai, W.-J., Hu, X., Gruber, N., Mackenzie, F. T., and Regnier, P.: Continental shelves as a variable but increasing global sink for atmospheric carbon dioxide, Nat Commun, 9, 454, https://doi.org/10.1038/s41467-017-02738-z, 2018.

Laws, E. A, Landry, M. R., Barber, R. T., Campbell, L., Dickson, M.-L., and Marra J.: Carbon cycling in primary production bottle incubations: Inferences from grazing experiments and photosynthetic studies using ^{14}C and ^{18}O in the Arabian Sea, Deep Sea Res Part II, 47, 1339-1352, https://doi.org/10.1016/S0967-0645(99)00146-0, 2000.

Lechtenfeld, O. J., Hertkorn, N., Shen, Y., Witt, M., and Benner, R.: Marine sequestration of carbon in bacterial metabolites, Nat Commun, 6, 6711, https://doi.org/10.1038/ncomms7711, 2015.

Lee, M.-H., Osburn, C. L., Shin, K.-H., and Hur, J.: New insight into the applicability of spectroscopic indices for dissolved organic matter (DOM) source discrimination in aquatic systems affected by biogeochemical processes, Water Res, 147, 164–176, https://doi.org/10.1016/j.watres.2018.09.048, 2018.

720   Lehahn, Y., d'Ovidio, F., and Koren, I.: A Satellite-Based Lagrangian View on Phytoplankton Dynamics, Ann
721   Rev Mar Sci, 10, 99–119, https://doi.org/10.1146/annurev-marine-121916-063204, 2018.

722   Lønborg, C., Álvarez-Salgado, X. A., Davidson, K., Martínez-García, S., and Teira, E.: Assessing the microbial
723   bioavailability and degradation rate constants of dissolved organic matter by fluorescence
724   spectroscopy in the coastal upwelling system of the Ría de Vigo, Mar Chem, 119, 121–129,
725   https://doi.org/10.1016/j.marchem.2010.02.001, 2010.

726   Lønborg, C., Yokokawa, T., Herndl, G. J., and Antón Álvarez-Salgado, X.: Production and degradation of
727   fluorescent dissolved organic matter in surface waters of the eastern north Atlantic ocean, Deep Sea
728   Res Part I: Oceanog Res Pap, 96, 28–37, https://doi.org/10.1016/j.dsr.2014.11.001, 2015.

729   Lucas, A. J., Guerrero, R. A., Mianzán, H. W., Acha, E. M., and Lasta, C. A.: Coastal oceanographic regimes
730   of the Northern Argentine Continental Shelf (34–43°S), Estuar Coast Shelf Sci, 65, 405–420,
731   https://doi.org/10.1016/j.ecss.2005.06.015, 2005.

732   Lund Paulsen, M., Müller, O., Larsen, A., Møller, E. F., Middelboe, M., Sejr, M. K., and Stedmon, C.:
733   Biological transformation of Arctic dissolved organic matter in a NE Greenland fjord, Limnol
734   Oceanogr, 64, 1014–1033, https://doi.org/10.1002/lno.11091, 2019.

735   McCauley, D. J., Gellner, G., Martinez, N. D., Williams, R. J., Sandin, S. A., Micheli, F., Mumby, P. J., and
736   McCann, K. S.: On the prevalence and dynamics of inverted trophic pyramids and otherwise top-heavy
737   communities, Ecol Lett, 21, 439–454, https://doi.org/10.1111/ele.12900, 2018.

738   McKnight, D. M., Boyer, E. W., Westerhoff, P. K., Doran, P. T., Kulbe, T., and Andersen, D. T.:
739   Spectrofluorometric characterization of dissolved organic matter for indication of precursor organic
740   material and aromaticity, Limnol Oceanogr, 46, 38–48, https://doi.org/10.4319/lo.2001.46.1.0038,
741   2001.

742   Moran, M. A., Ferrer-González, F. X., Fu, H., Nowinski, B., Olofsson, M., Powers, M. A., Schreier, J. E.,
743   Schroer, W. F., Smith, C. B. and Uchimiya, M.: The Ocean's labile DOC supply chain. Limnol
744   Oceanogr, 67, 1007-1021, https://doi.org/10.1002/lno.12053, 2022.

745   Nagata, T. and Kirchman, D.: Release of macromolecular organic complexes by heterotrophic marine
746   flagellates, Mar Ecol Prog Ser, 83, 233–240, https://doi.org/10.3354/meps083233, 1992.

747   Negri, R. M., Silva, R. I., Segura, V., and Cucchi Colleoni, A. D.: Estructura de la comunidad del fitoplancton
748   en el área de El Rincón, Mar Argentino (febrero 2011), Revista Investigación Desarrollo Pesquero, 23,
749   7–22, 2013.

750   Negri, R. M., Molinari, G., Carignan, M., Ortega, L., Ruiz, M. G., Cozzolino, E., Cucchi-Colleoni, A. D., Lutz,
751   V. A., Costagliola, M., Garcia, A. B., Izzo, S., Jurquiza, V., Salomone, A., Odizzio, M., La Torre, S.,
752   Sanabria, A., Hozbor, M. C., Peressutti, S. R., Méndez, S. M., Silva, R., Martínez, A., Cepeda, G. D.,
753   Viñas, M. D., Diaz, M. V., Pajaro, M., Mattera, M. B., Montoya, N. G., Berghoff, C., and Leonarduzzi,
754   E.: Ambiente y plancton en la zona Común de pesca argentino-uruguaya en un escenario de cambio
755   climático (marzo, 2014), Publicaciones de la Comisión Técnica Mixta del Frente Marítimo, 251–316,
756   2016.

Orselli, I. B. M., Kerr, R., Ito, R. G., Tavano, V. M., Mendes, C. R. B., and Garcia, C. A. E.: How fast is the Patagonian shelf-break acidifying?, J Mar Syst, 178, 1–14, https://doi.org/10.1016/j.jmarsys.2017.10.007, 2018.

Osburn, C. L., Kinsey, J. D., Bianchi, T. S., and Shields, M. R.: Formation of planktonic chromophoric dissolved organic matter in the ocean, Mar Chem, 209, 1–13, https://doi.org/10.1016/j.marchem.2018.11.010, 2019.

Porter, K. G. and Feig, Y. S.: The use of DAPI for identifying and counting aquatic microflora1, Limnol Oceanogr, 25, 943–948, https://doi.org/10.4319/lo.1980.25.5.0943, 1980.

Redfield, A. C., Ketchum, B. H., and Richards, F. A.: The influence of organisms on the composition of sea-water, in: The sea: ideas and observations on progress in the study of the seas, vol. 2, edited by: Hill, M. N., Wiley Interscience, New York, 26–77, 1963.

Romera-Castillo, C., Sarmento, H., Álvarez-Salgado, X. A., Gasol, J. M., and Marraséa, C.: Production of chromophoric dissolved organic matter by marine phytoplankton, Limnol Oceanogr, 55, 446–454, https://doi.org/10.4319/lo.2010.55.1.0446, 2010.

Romera-Castillo, C., Sarmento, H., Álvarez-Salgado, X. A., Gasol, J. M., and Marrasé, C.: Net production and consumption of fluorescent colored dissolved organic matter by natural bacterial assemblages growing on marine phytoplankton exudates, Appl Environ Microbiol, 77, 7490–7498, https://doi.org/10.1128/AEM.00200-11, 2011.

Romero, S. I., Piola, A. R., Charo, M., and Garcia, C. a. E.: Chlorophyll- a variability off Patagonia based on SeaWiFS data, J Geophys Res, 111, 1–11, https://doi.org/10.1029/2005JC003244, 2006.

Sanders, R., Caron, D., and Berninger U, G.: Relationships between bacteria and heterotrophic nanoplankton in marine and fresh waters: an inter-ecosystem comparison, Mar Ecol Prog Ser, 86, 1–14, https://doi.org/10.3354/meps086001, 1992.

Saraceno, M., Bodnariuk, N., Ruiz-Etcheverry, L. A., Berta, M., Simionato, C. G., Beron-Vera, F. J., and Olascoaga, M. J.: Lagrangian characterization of the southwestern Atlantic from a dense surface drifter deployment, Deep Sea Res Part I: Oceanog Res Pap, 208, 104319, https://doi.org/10.1016/j.dsr.2024.104319, 2024.

Sarmento, H., Morana, C., and Gasol, J. M.: Bacterioplankton niche partitioning in the use of phytoplankton-derived dissolved organic carbon: quantity is more important than quality, ISME J, 10, 2582–2592, https://doi.org/10.1038/ismej.2016.66, 2016.

Sherr, E. B. and Sherr, B. F.: Heterotrophic dinoflagellates: a significant component of microzooplankton biomass and major grazers of diatoms in the sea. Mar Ecol Prog Ser, 352, 187-197, https://doi:10.3354/meps07161, 2007.

Sieburth, J. McN., Smetacek, V., and Lenz, J.: Pelagic ecosystem structure: Heterotrophic compartments of the plankton and their relationship to plankton size fractions, Limnol Oceanogr, 23, 1256–1263, https://doi.org/10.4319/lo.1978.23.6.1256, 1978.

794 Silva, R., Negri, R., and Lutz, V.: Summer succession of ultraphytoplankton at the EPEA coastal station
795   (Northern Argentina), J Plankton Res, 31, 447–458, https://doi.org/10.1093/plankt/fbn128, 2009.

796 Simon, M. and Azam, F.: Protein content and protein synthesis rates of planktonic marine bacteria, Mar Ecol
797   Prog Ser, 51, 201–213, https://doi.org/10.3354/meps051201, 1989.

798 Skoog, A., Thomas, D., Lara, R., and Richter, K.-U.: Methodological investigations on DOC determinations by
799   the HTCO method, Mar Chem, 56, 39–44, https://doi.org/10.1016/S0304-4203(96)00084-9, 1997.

800 Spencer, R. G. M., Pellerin, B. A., Bergamaschi, B. A., Downing, B. D., Kraus, T. E. C., Smart, D. R., Dahlgren,
801   R. A., and Hernes, P. J.: Diurnal variability in riverine dissolved organic matter composition
802   determined by *in situ* optical measurement in the San Joaquin River (California, USA), Hydrol Process,
803   21, 3181–3189, https://doi.org/10.1002/hyp.6887, 2007.

804 Staniewski, M. A. and Short, S. M.: Potential viral stimulation of primary production observed during
805   experimental determinations of phytoplankton mortality. Aquat Microb Ecol, 71, 239-256,
806   https://doi.org/10.3354/ame01679, 2014.

807 Stedmon, C. A. and Bro, R.: Characterizing dissolved organic matter fluorescence with parallel factor analysis:
808   a tutorial, Limnol Oceanogr Methods, 6, 572–579, https://doi.org/10.4319/lom.2008.6.572, 2008.

809 Stedmon, C. A., Markager, S., and Bro, R.: Tracing dissolved organic matter in aquatic environments using a
810   new   approach   to   fluorescence   spectroscopy.   Mar   Chem,   82(3-4),   239-254,
811   https://doi.org/10.1016/S0304-4203(03)00072-0, 2003.

812 Suttle, C. A.: Viruses in the sea, Nature, 437, 356–361, https://doi.org/10.1038/nature04160, 2005.

813 Taylor, A. and Landry, M.: Phytoplankton biomass and size structure across trophic gradients in the southern
814   California   Current   and   adjacent   ocean   ecosystems,   Mar   Ecol   Prog   Ser,   592,   1–17,
815   https://doi.org/10.3354/meps12526, 2018.

816 Taylor, G. T., Iturriaga, R., and Sullivan, C. W.: Interactions of bactivorous grazers and heterotrophic bacteria
817   with   dissolved   organic   matter,   Mar   Ecol   Prog   Ser,   60,   1884–1888,
818   https://doi.org/10.3354/meps023129, 1985.

819 Tremaine, S. C. and Mills, A. L.: Tests of the critical assumptions of the dilution method for estimating
820   bacterivory   by   microeucaryotes,   Appl   Environ   Microbiol,   53,   2914–2921,
821   https://doi.org/10.1128/aem.53.12.2914-2921.1987, 1987.

822 Urban-Rich, J., McCarty, J. T., and Shailer, M.: Effects of food concentration and diet on chromophoric
823   dissolved organic matter accumulation and fluorescent composition during grazing experiments with
824   the   copepod   Calanus   finmarchicus,   ICES   J   Mar   Sci,   61,   542–551,
825   https://doi.org/10.1016/j.icesjms.2004.03.024, 2004.

826 Weinbauer, M. G. and Peduzzi, P.: Significance of viruses versus heterotrophic nanoflagellates for controlling
827   bacterial   abundance   in   the   northern   Adriatic   Sea,   J   Plankton   Res,   17,   1851–1856,
828   https://doi.org/10.1093/plankt/17.9.1851, 1995.